# Influence of Unsteady Mass Transfer on Dynamics of Rising and Sinking Droplet in Water: Experimental and CFD Study

**Abhijit Rao, Rupesh K. Reddy, Kalliat T. Valsaraj, and Krishnaswamy Nandakumar**
Cain Dept. of Chemical Engineering, Louisiana State University, Baton Rouge, LA 70802

**Shashank Pandey**
Dept. of Chemical Engineering, Indian Institute of Technology, Kharagpur, West Bengal 721302 India

**Chunliang Wu**
ANSYS Inc., Houston, TX 77094

*DOI 10.1002/aic.14612*
*Published online September 23, 2014 in Wiley Online Library (wileyonlinelibrary.com)*

*Experimental and numerical investigations were conducted to study the effect of unsteady mass transfer on the dynamics of an organic droplet released in quiescent water. The situation is important and relevant to deep sea oil spill scenario. The droplet contains two components, one is heavier (immiscible) than water and other is lighter (miscible). When released, with an initial mixture density (890–975 kg/m$^3$) lower than that of surrounding water, droplet rises in the column. The mass transfer of lighter solute component into water causes the droplet density to increase and droplet sinks when the density exceeds that of water. A mass-transfer correlation accounting for the loss of the solute, based on Reynolds, Grashoff, and Schmidt numbers was developed. A two-dimensional axisymmetric Computational Fluid Dynamics (CFD) model accounting for species transport was developed to emulate the experimental observations. The study also helped in identifying dominant mass-transfer mechanisms during different stages of droplet motion.* © 2014 American Institute of Chemical Engineers *AIChE J*, 61: 342–354, 2015
*Keywords: mass-transfer coefficient, unsteady mass transfer, computational fluid dynamics, volume of fluid, droplet dynamics, transport processes*

## Introduction

Liquid droplets form the most fundamental entity in many physical systems of industrial importance. The occurrence of mass transfer to and from droplets driven by buoyancy can be found in applications such as liquid–liquid extraction, and during the environmental hazards such as deep water oil spills. The oil droplets entering the oceanic environment during an accidental release contain plethora of hydrocarbons, many of which are soluble in the ambient water. As reported by Yvon et al.,[1] there exists a strong evidence that in case of deep oil spills many readily soluble species fail to reach the surface. So, accounting for mass transfer of hydrocarbons is important in such situations.

Droplets are often referred to as a dispersed phase, which travel in an immiscible or partially miscible medium, the continuous phase. Studying fluid dynamics pertaining to a droplet becomes important as the predicted flow patterns can potentially offer help in explaining the factors which influence the overall mass-transfer process in the system. Sound understanding of fluid dynamics and thereby mass transfer in a single droplet can serve in estimating total mass transfer in a system with a swarm of droplets.

The motion of an immiscible droplet traveling in the stagnant medium draws a special interest due to the complex dynamics associated with it. Unlike rigid particle, the fluid droplet bears a deformable interface which allows for the exchange of momentum with the surrounding medium as it moves in the continuous phase. The shear at interface leads to the development of internal circulations, the strength of which depends on factors such as the viscosity ratio between the dispersed and continuous phase, the degree of contamination and so on.[2–4] The mass transfer occurs when concentration gradients exist in a medium; solute being transported from a region of higher to lower concentration. The interfacial mass transfer depends on the flow patterns inside as well as outside the droplet. The local diffusivities and advective currents control the movement of the solute in the system. Depending on the diffusivities of solute in dispersed ($D_{i,\mathrm{d}}$) and continuous ($D_{i,\mathrm{c}}$) phase, the mass-transfer rate is said to be controlled by dispersed phase when $D_{i,\mathrm{c}} \gg D_{i,\mathrm{d}}$. Resistance to mass transfer lies in continuous phase when $D_{i,\mathrm{d}} \gg D_{i,\mathrm{c}}$ and finally problem is referred to as conjugate problem when $D_{i,\mathrm{c}} \sim D_{i,\mathrm{d}}$. The subscript "i" represents the solute, "c" and "d" represent the solvents that comprise continuous and dispersed phases, respectively.

Many theoretical,[5–7] experimental,[8–11] and numerical[12,13] investigations have been carried out to gain good

Correspondence concerning this article should be addressed to K. Nandakumar at nandakumar@lsu.edu.

understanding of mass-transfer process occurring to and from a moving single droplet. Skelland and Wellek[14] experimentally studied the mass-transfer process for solute, moving into falling oscillating and nonoscillating droplets, considering the resistance to mass transfer to lie in dispersed phase. Garner et al.[15] examined the importance of circulations inside the droplet and measured mass-transfer coefficients in systems with droplets in which circulations were significant. To ensure this, they used systems with very low interfacial tensions. They found that mass transfer for stagnant droplet could be correlated with $Re^{\frac{1}{2}}Sc^{\frac{1}{3}}$, whereas for circulating droplets it was $Re^{\frac{1}{2}}Sc^{\frac{1}{2}}$.

The theoretical work for mass transfer has been carried out for creeping and potential flow[2,16] conditions for which the analytical solutions are available. For complicated flow profiles, numerical methods are preferred which are based on obtaining solutions to Navier–Stokes equation and species convection–diffusion equation. Apart from concentration gradients, the effective mass-transfer rate also depends on the interfacial area available for the solute transport. Hence, for a successful modeling of mass-transfer process by numerical means, it is essential to correctly resolve transient evolution of the interface under prevailing conditions. Many methods have been used by authors to capture interface in a multiphase system viz. Volume of fluid (VOF) method,[17] Marker and cell method,[18] Front Tracking Method,[19] Level Set Method,[20] and so on.

Deshpande and Zimmerman[13] used level set method to track the motion of buoyancy driven droplet and carried out mass-transfer simulation by solving concentration convection–diffusion equation and governing equations of level set scheme separately, that is, the mass transport equation was solved using the velocity field obtained from flow equations. The mass-transfer coefficients obtained from the simulation were found to be of same order of magnitude with those evaluated using empirical correlations. Wang et al.[21] also used level set method for capturing interface but solved the flow and species equations simultaneously in a moving reference frame with respect to droplet. The results from numerical model were found to agree well with their experimental data.

Mass transfer from deformable droplets to continuous phase was studied by Petera and Weatherley,[22] in which a falling droplet was modeled using modified Lagrange–Galerkin finite element method. They adopted the remeshing algorithm to maintain a fine density of mesh near the interface of the droplet. In a more recent work, Marschall et al.[23] demonstrated implementation of mass transfer using finite volume method employing continuous species transport method to account for concentration jump at the interface. This model was built on lines of continuum surface force (CSF) model suggested by Brackbill et al.[24] A pseudo-VOF method was used for interface capturing.

In another interesting work, Adekojo Waheed et al.[25] have discussed the significance of combined forced and free convection for the mass transfer at lower $Re$ for a conjugate problem. From their numerical simulations which were based on finite element formulation, they were able to reaffirm the fact that the mass transfer is highly dependent on flow conditions. Paschedag et al.,[26] in their work, identified set of parameters viz. $Re$, $Pe$, $\mu^*$, and $D^*$ which dictate the mass transfer and carried out study on sensitivity of these parameters on $Sh$.

### *Outline*

During the "Deepwater Horizon" accident in the deep sea in 2010, about 4.9 million barrels of oil[27] was released (point of release was at the depth of around 5000 feet) into the Gulf of Mexico, making the spill one of the worst subsurface spills in recent times. Unlike with surface spills, in deep water spills, the droplets generated by the shear interaction between the oil emanating from oil well and surrounding ocean water, spend larger amount of time in the water column. The introduction of these alien hydrocarbons in the marine environment can be detrimental to the existence of the aquatic life. The complex mechanisms that occur in the deep water oil spill where the dissolved lighter hydrocarbons in the oil are eventually transferred to the sea water, is one of the motivations for this study. In this study, we focus on the mass transfer, however, in reality many other coupled mechanisms such as gas release with decreasing hydrostatic head, surfactant effects on mass transfer and interaction with suspended marine particulate matter that may result in eventual sinking of droplet, are all important.[28] The oil droplets can be assumed as a pseudo binary mixture,[29] the first component includes all lighter hydrocarbons which are soluble in the surrounding water and the second component represents all heavier hydrocarbons practically insoluble in water. In this study, we have substituted the actual oil droplet with a binary organic mixture containing soluble and insoluble components.

In this work, we have investigated the effect of transient mass transfer on the dynamics of an organic droplet traveling in the quiescent water column, experimentally as well as numerically. Most of the researchers have studied mass transfer in a system where the droplet either ascends or descends in the continuous medium. However, in this experiment, it was observed that, with occurrence of mass transfer the droplet ascended in the water column initially, became stationary and then descended. This provided us an opportunity to explore different mechanisms which dictate the mass transfer of solute at various stages of the droplet motion. A mass-transfer correlation capable of accounting for the observed mass transfer was also developed by proposing a model based on first principles. A two-dimensional (2-D) axisymmetric numerical model based on the finite volume method which used VOF[17] with an interface reconstruction technique based on Piecewise Linear Interface Calculation (PLIC) representation for tracking the water-organic droplet interface was developed to gain insight on the changing flow patterns in the droplet as it encountered deceleration and acceleration during its motion.

The organic droplet consists of two components; a lighter soluble component, acetonitrile which has a density less than that of water and a heavier component, chlorobenzene, which is immiscible in water. The droplet released into the water column initially rises due to the buoyancy available to it. Due to the existing concentration gradient, acetonitrile is transferred from the droplet phase to the continuous phase, causing its density to increase over a period of time. The droplet starts decelerating and reaches a stationary stage when its effective density becomes equal to that of the surrounding water. Further loss in acetonitrile allows the droplet to sink in the column. A typical trajectory assumed by a droplet in the experiment is shown in Figure 1.

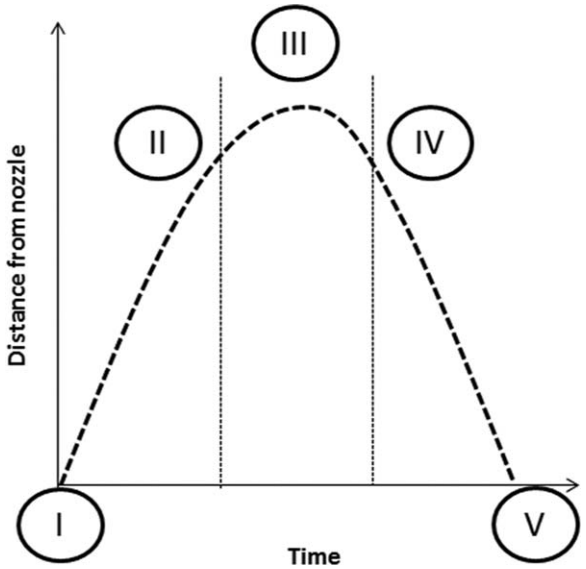


**Figure 1. The droplet motion in water column I to III represents ascent stage, III corresponds to stationary stage, III to V marks the descent stage.**

It is essential to note that due to continuous mass transfer of solute, the droplet never attains a terminal velocity; it either finds itself under acceleration or deceleration. Figure 2b shows the forces acting on the droplet in ascent and descent stages. The mass transfer of acetonitrile begins at the instant when the organic phase comes in contact with water. The loss of acetonitrile occurs during:

- Droplet formation
- Ascent stage
- Stationary stage
- Decent stage

The mass transfer occuring during the droplet formation depends on the rate at which it is introduced; which influences the flow patterns developing inside the droplet.[11] The slow formation of droplet eliminates the generation of internal circulations and the mass transfer can be described by means of diffusion. A fast formation rate causes generation of convection currents inside the droplet phase which enhances mass transfer. Several authors have reported that generated currents bring about enhancement of mass-transfer process.[30–33] The mass-transfer coefficients are highest at the intial stages of droplet formation[30] when circulations are vigourous and decay significantly with time when the circulations dampen out or die completely. Humphrey et al.[11] suggested a parameter called circulation number $Ci$ given by

$$Ci = We \cdot Re \tag{1}$$

to depict the transition of flow patterns from circulating to stagnate pattern during the evolution of the droplet. $Ci$ has highest value in the initial stages of formation and reaches a minimum value at the time of detachment. In the present study, the time taken for droplet formation was less than 10% of the total time spent by the droplet in the water column. This work does not focus on the mass transfer occuring during the droplet formation rather it explores the unsteady mass transfer that occurs after the droplet pinch off. Thus, the actual droplet formation and allied mass-transfer process was not included in the numerical model. However, the loss of the solute, acetonitrile, was accounted for by estimating the composition of droplet at the time of pinch off through an optimization procedure described in later sections.

The article is organized as follows. The next section describes the experimental setup and the methodology. This is followed by a section that contains a brief discussion on the numerical model developed to emulate the experimental observations. It covers the governing equations followed by a section depicting the implementation of the mass-transfer process in the model. Next, we describe the procedure followed to obtain a mass-transfer correlation capable of describing the mass lost during the motion of droplet in the water column. In later sections, we have highlighted the role of natural convection in controlling mass transfer when droplet becomes stationary. It is followed by a discussion on key observations from the experiment and the results obtained from the numerical model.

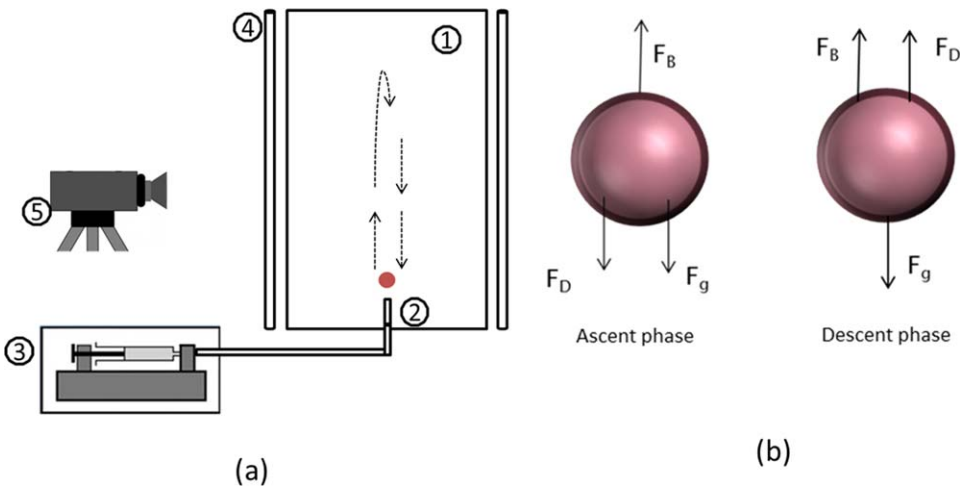


**Figure 2. (a) Schematic representation of experimental setup (1) glass tank with stagnant water, (2) borosilicate nozzle, (3) syringe pump, (4) illumination system, and (5) high speed camera. (b) Body forces acting on the droplet during ascent and descent stages.**

**[Color figure can be viewed in the online issue, which is available at wileyonlinelibrary.com.]**

Table 1. Physical Properties @ 25 °C of the Materials Used

| | Density ($kg/m^3$) | Viscosity (kg/m s) |
|---|---|---|
| Dispersed Phase | | |
| Acetonitrile | 791 | 0.000343 |
| Chlorobenzene | 1104 | 0.00073 |
| Continuous Phase | | |
| Water | 999.5 | 0.001 |
| Properties | | |
| Interfacial Tension (mN/m) | | 36 |
| Dispersed phase Diffusivity $D_{i,d}$ ($m^2/s$) | | $1.14\times10^{-9}$ |
| Continuous phase diffusivity $D_{i,c}$ ($m^2/s$) | | $1.43\times10^{-9}$ |

## Experimental

The dispersed phase, composed of a mixture of acetonitrile and chlorobenzene with former being a solute, travels in the continuous phase, water (free of acetonitrile). The composition of solute in dispersed phase ensures that the emerging droplet is buoyant than the surrounding medium. The solute transfer from dispersed phase to continuous phase occurs under existing concentration gradients. Acetonitrile (95%) supplied by Sigma Aldrich® and 99% chlorobenzene from Alfa Aesar® were used in the experiment. The properties of these materials can be found in Table 1. The experimental setup consists of a vertical rectangular column made of glass, with dimensions $50\times60\times40$ $cm^3$, filled with water. The assembly of all major components has been shown in Figure 2a. The dispersed phase was released into the stagnant pool of water through nozzle made up of borosilicate glass, with the help of a high precision syringe pump. A long PTFE (teflon) tube was used to connect the syringe mounted on syringe pump and the well machined nozzle having an internal diameter (ID) of 2 mm. The outer wall of the nozzle was passivated to reduce the wettability by organic mixture and thereby it allowed for the smooth and efficient evolution of the droplet. The dimension of the tank was far greater than that of droplet which ensured that the effect of the walls on the dynamics of droplets was minimal.

The organic droplet consists of a miscible component (acetonitrile) and an immiscible component (chlorobenzene). When it is released in tank containing water, with an initial mixture density less than that of the surrounding medium, it rises in the column. The mass transfer of lighter solute component from dispersed phase to the continuous phase causes the density of droplet to increase gradually, which causes droplet to decelerate, reach a stationary state and eventually sink when its density exceeds that of water. The dispersed phase was introduced at a very small flow rate. To ensure that only a single droplet was released at a time, the pump was switched off as soon as the droplet detached from the nozzle. Four sets of experiments were conducted for droplets with various initial mixture densities; the details have been provided in Table 2. Before each run, the tank was scrupulously cleaned and the water was replaced.

The images of droplets were captured using a high speed camera, Canon® EX-ZR200, capable of capturing multiple images at the shutter speed of 1/1000 s at 30 frames per second. The system was illuminated using 60 W fluorescent lamps kept at the corners of the tank. A background sheet was placed to improve the quality of images. The processing of images was done by subtracting the background and converting it into a binary image using a threshold feature available in ImageJ®. The densities of the continuous and dispersed phases were measured at the beginning of each run. The diameter of the organic droplet was estimated from the sequence of images taken near the tip of the nozzle, at the time when the droplet was about to pinch off from the nozzle. The measurements were done for 20 droplets and the average value was calculated. The trajectory data of the droplet were extracted using the high definition video captured from the camera. A graduated measuring scale was part of the experimental setup and during image processing the number of pixels for a known distance was determined and this was used for evaluating the droplet size and its position.

## Numerical Model

In this section, we present the numerical model which accounts for the mass-transfer process and thereby predicts the trajectory of the droplet observed in the experiment. The model was built within an Eulerian framework using commercially available finite volume CFD code, ANSYS Fluent®. It was observed in the experiment that motion of droplet during ascent and descent stages, was rectilinear and the deviation of the droplet from the plane of nozzle was negligible. These observations substantiate the fact that in the present case, lift forces in the present case are negligible. So, in order to save on the computational effort, in this study, we have considered the flow around the droplet to be axisymmetric. The other assumptions that go into the model are:

- The fluids are Newtonian, incompressible, and viscous.
- Isothermal conditions prevail.
- Mass transfer has no effect on the properties of the system.
- The interfacial tension is assumed to be constant and the influence of the solute mass transfer on interfacial tension has not been considered. No surface active agents are present in the present experiments.

### *Governing equations*

The continuity and momentum equations under axisymmetric assumption can be written as

$$\frac{\partial\rho}{\partial t}+\frac{\partial}{\partial z}(\rho v_z)+\frac{\partial}{\partial r}(\rho v_r)+\frac{\rho v_r}{r}=0 \tag{2}$$

$$\begin{aligned}\frac{\partial}{\partial t}(\rho v_z)+\frac{1}{r}\frac{\partial}{\partial z}(r\rho v_r v_z)+\frac{1}{r}\frac{\partial}{\partial r}(r\rho v_r v_z)\\ =-\frac{\partial p}{\partial z}+\frac{1}{r}\frac{\partial}{\partial z}\left[r\mu\left(2\frac{\partial v_z}{\partial z}-\frac{2}{3}(\nabla\cdot\vec{v})\right)\right]\\ +\frac{1}{r}\frac{\partial}{\partial r}\left[r\mu\left(\frac{\partial v_z}{\partial r}+\frac{\partial v_r}{\partial z}\right)\right]+\rho\vec{g}+F_z\end{aligned} \tag{3a}$$

$$\begin{aligned}\frac{\partial}{\partial t}(\rho v_r)+\frac{1}{r}\frac{\partial}{\partial z}(r\rho v_r v_z)+\frac{1}{r}\frac{\partial}{\partial r}(r\rho v_r v_z)\\ =-\frac{\partial p}{\partial r}+\frac{1}{r}\frac{\partial}{\partial z}\left[r\mu\left(\frac{\partial v_z}{\partial r}+\frac{\partial v_r}{\partial z}\right)\right]\\ +\frac{1}{r}\frac{\partial}{\partial r}\left[r\mu\left(2\frac{\partial v_r}{\partial r}-\frac{2}{3}(\nabla\cdot\vec{v})\right)\right]\\ -2\mu\frac{v_r}{r^2}+\frac{2}{3}\frac{\mu}{r}(\nabla\cdot\vec{v})\ +\ F_r\end{aligned} \tag{3b}$$

where $\nabla\cdot\vec{v}=\frac{\partial v_z}{\partial z}+\frac{\partial v_r}{\partial r}+\frac{v_r}{r}$

Equations 2 and 3 represent the $z$ and $r$ component momentum equations, respectively. $\boldsymbol{F}$ accounts for the body

Table 2. Details of the Droplets Found in the Experiment

| Experiment # | Initial Mixture Density (Experiment) (kg/m$^3$) | Droplet Diameter (mm) | Time for Droplet Formation (s) | Mass Fraction of Acetonitrile at Time Off Pinch Off from Model ($x_0$) |
|---|---|---|---|---|
| 1 | 890 | 3.30 | 0.50 | 0.48 |
| 2 | 920 | 4.10 | 0.77 | 0.39 |
| 3 | 950 | 4.65 | 0.95 | 0.34 |
| 4 | 975 | 4.90 | 1.00 | 0.32 |

forces; in current case, it refers to volumetric force due to interfacial tension, which is calculated according CSF model[24] given by

$$F=\sigma\frac{\rho\gamma\nabla\alpha}{\langle\rho\rangle} \tag{4}$$

where $\sigma$ is surface tension coefficient, $\gamma$ is local surface curvature given by

$$\gamma=\nabla\cdot\hat{n} \tag{5a}$$

with $\hat{n}$ being unit surface normal vector which can be written in terms of volume fraction function as

$$\hat{n}=\frac{\nabla\alpha}{|\nabla\alpha|} \tag{5b}$$

The accuracy of the volumetric interfacial tension force described by Eq. 4 depends on the proper evaluation of the curvature. In this study, we have used the VOF gradients directly from the nodes which are conjugated with node-based smoothing of VOF field for accurate evaluation of the curvature.

In present study, VOF method[17] has been used to capture interface between the continuous phase and the dispersed phase. The interface is constructed using piecewise linear (PLIC) approach suggested by Young.[34] VOF is advantageous over other methods for they are relatively simple, robust, accurate, and account for substantial topological changes in the interface.[35] The VOF method defines a single momentum equation (Eqs. 3a and 3b) which is shared by both phases. It is solved along with the continuity equation (Eq. 2) to yield the velocity field. The method is naturally conservative, has a fast convergence and a reasonable accuracy.[36] The VOF method works on a fixed grid and the position of interface is determined by the solution of a scalar balance equation for the volume fraction $\alpha$ of dispersed phase. For $q$th phase

$$\frac{\partial\alpha_q}{\partial t}+\nabla\cdot\left(\vec{v}\alpha_q\right)=\frac{S}{\rho_q} \tag{6}$$

$\alpha=0$ in continuous phase and $\alpha=1$ in dispersed phase. The smeared region with $\alpha$ taking values between 0 and 1 represents the interface. The term on the R.H.S accounts for the change in the interface position due to the mass transfer. "$S$" is the volumetric mass-transfer rate which represents exchange of mass (solute) between the dispersed and the continuous phase.

The convective transport of solute in the stagnant systems depends on flow fields generated by buoyancy of droplet which is attributed to the density difference between two phases. The evolution of concentration fields of acetonitrile in the continuous and dispersed phases is tracked by including species transport equation. In computational cells where interface is located, following species transport equation is applicable

$$\frac{\partial c_i}{\partial t}+\vec{v}\cdot\nabla c_i=-D_{ij}\nabla^2 c_i+S \tag{7}$$

$c_i$ is the concentration of the acetonitrile (represented by subscript "$i$") and $D_{ij}$ represents the molecular diffusivity in corresponding phases(denoted by subscript "$j$"). The convective term in Eq. 7 is evaluated using the velocity field obtained after solving the continuity and momentum equations. It is important to note that "$S$" is invoked in the cells through which the interface passes. "$S$" takes a value of 0 in rest of the domain.

### *Implementation of mass transfer in ANSYS Fluent®*

The mass transfer has been facilitated in the model using user-defined functions feature in Fluent®. In ANSYS Fluent® mass transfer between the phases is achieved by specifying the volumetric mass-transfer rate at which solute needs to be transferred from dispersed to continuous phase. To implement this, one of the foremost steps is to identify the cells that constitute the interface ($0<\alpha<1$). In finite volume method, it is essential to specify a source term in volumetric sense and a volumetric mass-transfer rate is specified in these cells

$$S=\frac{k_l A_\mathrm{d}(c_{i,\mathrm{d}}-c_{i,\mathrm{c}})}{V_i} \tag{8}$$

$S$ represents the volumetric mass rate (kg/m$^3$s), which depends on the instantaneous mass transfer coefficient $k_l$, surface area of droplet $A_\mathrm{d}$, and the concentration difference of acetonitrile between the dispersed phase and the continuous phase. $V_i$ is the total volume occupied by the dispersed phase in the computational cells through which the interface passes. In this study, the effect of compositional changes on $k_l$ has been taken into consideration. The value of $k_l$ depends on $Re$ of droplet. More details on estimation of $k_l$ has been described later in this article. During each iteration, average concentration of acetonitrile is computed. Using the value of $k_l$, $S$ can be evaluated from Eq. 8 and is applied at the computational cells through which the interface passes.

### *Numerical methods and simulation setup*

The transient simulation was carried out using the explicit scheme. The explicit scheme is advantageous as it renders a clear, crisp interface without numerical diffusion. The pressure velocity coupling was established using pressure-implicit with the splitting of operators algorithm. The spatial discretization used in momentum equation was the second-order upwind differencing scheme. The calculation of gradients was based on the Green–Gauss Cell-Based method. Pressure staggering option scheme was used for pressure interpolation. The geometric reconstruction scheme was used for constructing interfaces in the cells where $\alpha$ varied between 0 and 1 (representing interface).

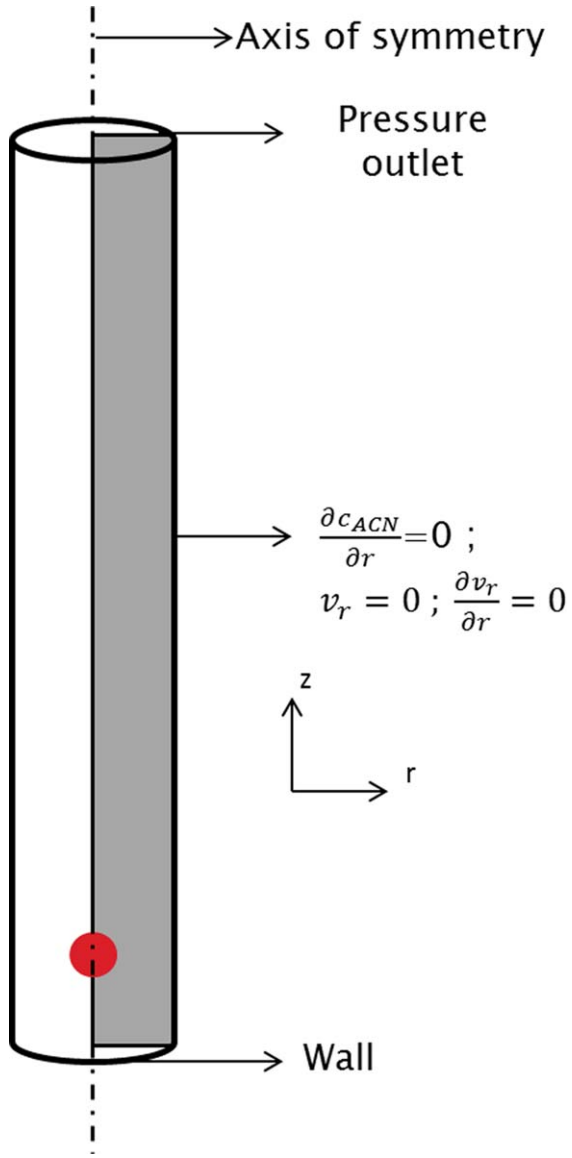


**Figure 3. Computational domain and boundary conditions for 2-D axisymmetric simulation.**

**[Color figure can be viewed in the online issue, which is available at wileyonlinelibrary.com.]**

The computational domain consists of a small section $\Omega=[(x,y) : 0 \le x \le 60R, 0 \le y \le 15R]$, where $R$ refers to the radius of the droplet. The 2-D axisymmetric computational domain (shaded region in Figure 3) and the boundary conditions used in the simulation are depicted in Figure 3. The wall boundary condition imposes no slip (both components of velocities are zero) at the lower face of the computational domain

$$v_r, v_z=0;\ \ c_i=0 \tag{9a}$$

The assumption of axisymmetry implies that there are no circumferential gradients in the flow. Thus

$$v_\theta=0;\ \frac{\partial v_r}{\partial \theta}=0;\ \frac{\partial v_z}{\partial \theta}=0 \quad \text{and} \quad \frac{\partial c_i}{\partial \theta}=0 \tag{9b}$$

At the boundary of computational domain, symmetric boundary conditions (terminology used in ANSYS Fluent®) are imposed, which ensures that at the normal component of velocities is zero and the normal gradients of all other quantities are zero

$$v_r=0;\ \frac{dc_i}{dr}=0 \tag{9c}$$

At the top surface, pressure outlet boundary condition is applied which implies

$$\frac{\partial v_r}{\partial z}=0;\ \frac{dc_i}{dz}=0 \tag{9d}$$

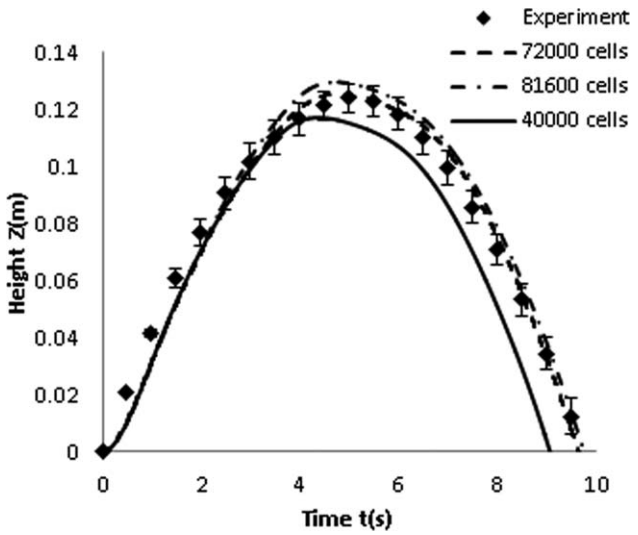


**Figure 4. Mesh dependency test; initial droplet density 970 kg/m$^3$.**

ANSYS ICEM® was used to build the mesh containing quadrilateral elements over the domain. The mesh dependency test was performed with meshes containing 40,000, 72,000, and 81,600 elements. The mesh was finer in the region near to the axis where droplet motion is expected. The grid resolution results are shown in Figure 4 and Table 3. The variation in results with grid resolution $1.85\times10^{-4}$ and $1.65\times10^{-4}$ was under 3% and the former mesh resolution was used for performing simulations. The time stepping was chosen to keep the global Courant number less than 0.25. The simulation was carried out on eight processors using a supercomputing facility at HPC, in LSU.

## Estimation of Mass-Transfer Coefficient

When the droplet is in motion, the convection currents around the droplet affect the mass-transfer rate. The mechanisms of mass transfer at various stages of droplet motion are summarized in Table 4. As shown in Figure 1, forced convection dominates the mass-transfer process in the regions between I to II and IV and V. Mass-transfer process occurs by a combined mechanism in the regions II to III and III to IV, when both forced and natural convection control mass transfer. When droplet comes to rest (region III), mass-transfer process is attributed to diffusion and natural convection. More details on this have been provided in the later sections of this article.

Mass-transfer correlation has been developed using a model based on first principles described in Appendix. The chief assumptions that go into the model are:

- Droplet remains spherical.
- The droplet follows a rectilinear path.

**Table 3. Mesh Dependency Test**

| # of Cells in Domain | Grid Resolution Within the Droplet (cm) | Height Reached by Droplet (cm) | Time to Reach Highest Position $t_{highest}$ (s) | Time at the End of Descent Stage $t_{final}$ (s) |
|---|---|---|---|---|
| 40,000 | $4.08 \times 10^{-4}$ | 11.71 | 4.37 | 9.08 |
| 72,000 | $1.85 \times 10^{-4}$ | 12.53 | 4.75 | 9.66 |
| 81,600 | $1.65 \times 10^{-4}$ | 12.95 | 4.69 | 9.76 |

Both the assumptions have been found to be valid in our experimental observations. The mass-transfer correlation has a form represented by Eq. 10 for the most part of ascent and descent stage when forced convection is significant and influences overall mass transfer. Equation 11 is valid when droplet passes through the stationary stage

$$Sh = A + G \quad Re^h Sc^i \tag{10}$$

$$Sh = A + B \quad Gr^c Sc^d + D \quad Re^e Sc^f \tag{11}$$

The first term on right-hand side represents the diffusion term which has a numerical value of 2, a limiting value suggested by Langmuir[37] when no fluid motion exists. The second term involving $Re$ accounts for the contribution of forced convection on mass transfer. The forced convection depends on the relative motion between the drop and the continuous phase. The natural convection becomes important when the droplet approaches the stationary state, as $Re$ (which depends on the droplet composition) falls to a low value.[25] The second term in Eq. 11 consisting of $Gr$ and $Sc$ represents the natural convection; where buoyancy effects manifest in $Gr$. The origin and significance of natural convection will be discussed in the later sections. At any instant of time, the average droplet velocity is used for evaluating $Re$. The definitions of all dimensionless numbers can be found at the end of this article.

To estimate the parameters in Eqs. 10 and 11, initially a guess value for each of them is supplied to solve the ordinary differential equations (ODE's) (given in Appendix) describing the motion of the droplet. The integrated trajectory profile is compared with the one observed in the experiment. An objective function $E$ expressing the error between the two profiles is constructed

$$E = \left( \frac{Z_{exp} - Z_{num}}{Z_{exp}} \right)^2 \tag{12}$$

where $Z_{exp}$ represents the location of droplet observed in the experiment at particular instant of time and $Z_{num}$ represents the corresponding value predicted from the solutions to the ODE's. The objective function $E = E(B, G, c, d, e, f, h, i, x_0)$ is dependent on all previously mentioned parameters. Here, $x_0$ is the mass fraction of acetonitrile at the instant when droplet pinches off from the nozzle. The objective function is then minimized to yield appropriate values of all parameters using a multivariable constrained optimization function "fmincon" available in MATLAB®. The sequence followed for evaluation of parameters has been shown in Figure 5.

The correlation obtained after following the minimization procedure were

$$Sh = 2 + 0.4\ Gr^{0.28} Sc^{0.31} + 0.213 Re^{0.45} Sc^{0.31} \quad \text{for } Re < 20 \tag{13}$$

$$Sh = 2 + 0.573 Re^{0.31} Sc^{0.44} \quad \text{for } Re > 20 \tag{14}$$

Depending on the instantaneous $Re$, the overall mass-transfer coefficient can be evaluated using the above correlations. The calculated value of mass-transfer coefficient falls in the range $1.7 \times 10^{-6}$– $4 \times 10^{-5}$ m/s which is comparable to the values found in literature, for similar systems. The correlations are valid in the regime observed in this experiment where the value of $Sc$ was around 800 and $Re$ was less than 200. Further, the correlations were used to predict the overall mass-transfer coefficient for the system described in Wang et al.[21] and the values obtained were in the same order as observed in their experiment. As the system exhibits high $Sc$, which corresponds to high $Pe$ ($Pe = Re \cdot Sc$), any convection induced near the interface should influence the mass transfer rate strongly. It has been stated earlier that the droplet loses acetonitrile during its formation, so the mixture composition $x_0$ at the time when droplet pinches off is expected to be different from its initial value at the time of injection. The value for $x_0$ has been obtained by treating it as an additional parameter (see Table 2); the error minimization sequence yields a more reliable estimate. The droplet becomes stationary when its density is equal to that of surrounding water and the corresponding mass fraction of acetonitrile at this point is 0.2642.

**Table 4. Mechanism of Mass Transfer During Different Stages of Droplet**

| Region in Figure 1 | Mechanism of Mass Transfer |
|---|---|
| I -> II and IV -> V | Diffusion + Forced Convection |
| II -> III and III -> IV | Diffusion + Forced Convection + Natural Convection |
| III | Diffusion + Natural Convection |

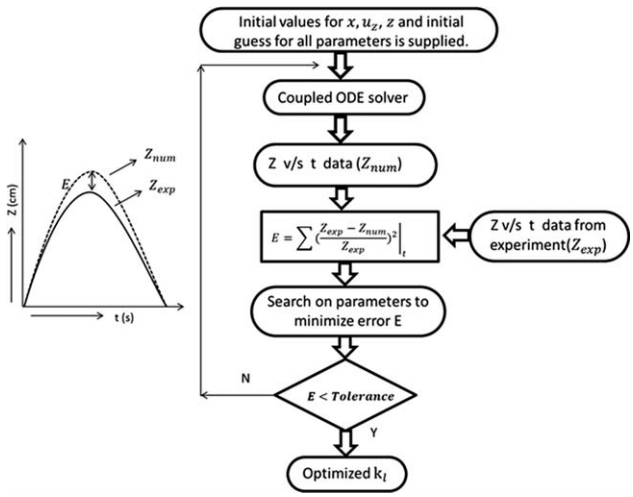


**Figure 5. Steps undertaken for optimizing parameters to estimate mass-transfer coefficient.**

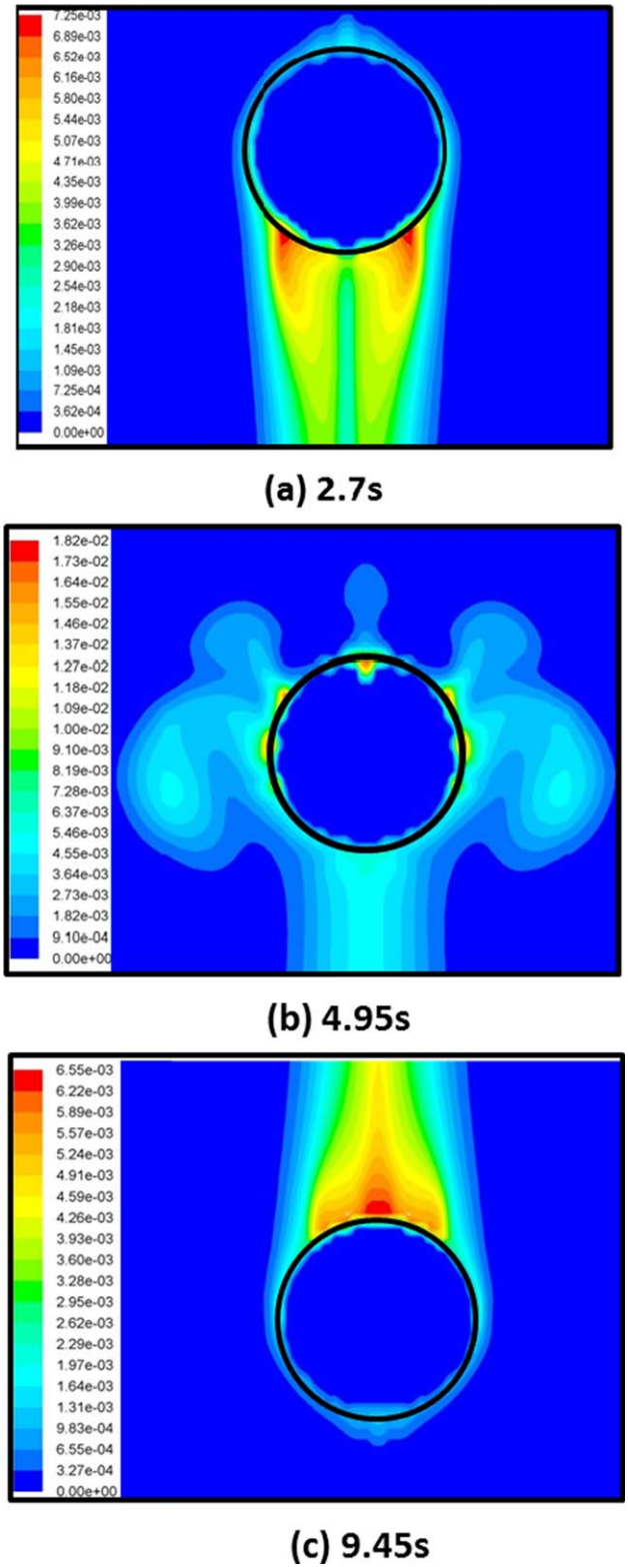


**Figure 6. Mass fraction of acetonitrile in continuous during (a) ascent stage, (b) stationary stage, and (c) descent stage from CFD simulations.**

**[Color figure can be viewed in the online issue, which is available at wileyonlinelibrary.com.]**

## Importance of Combined Transfer

In this section, we will examine the importance of the combined mass transfer mechanism which is predominant at low $Re$.[25] The acetonitrile moving out of the droplet dissolves in the surrounding water forms a mixture which is slightly less dense than that of water and rises in the column due to buoyancy. During the ascent stage of the droplet, the droplet travels with appreciable velocity and flow around the droplet forces the acetonitrile-water mixture to accumulate at rear end of the droplet (Figure 6a). The mass-transfer process during this stage of droplet motion is governed by forced convection (Eq. 14). However, when the droplet approaches stationary stage, it slows down, and the velocity of the surrounding acetonitrile-water mixture becomes comparable to that of droplet and hence the mass-transfer process is influenced by both natural as well as forced convection (Eq. 13). When a droplet comes to rest, the acetonitrile-water mixture interacts with the stationary droplet and enhances mass transfer and hence in this stage, natural convection governs the mass-transfer process. Contour plot corresponding to $t = 4.95$ s represents the stationary stage (Figure 6b). Forced convection again becomes predominant during the descent stage of the droplet which is accompanied by accumulation of acetonitrile-water mixture behind the droplet (Figure 6c). More details on this can be found in concluding part of the article.

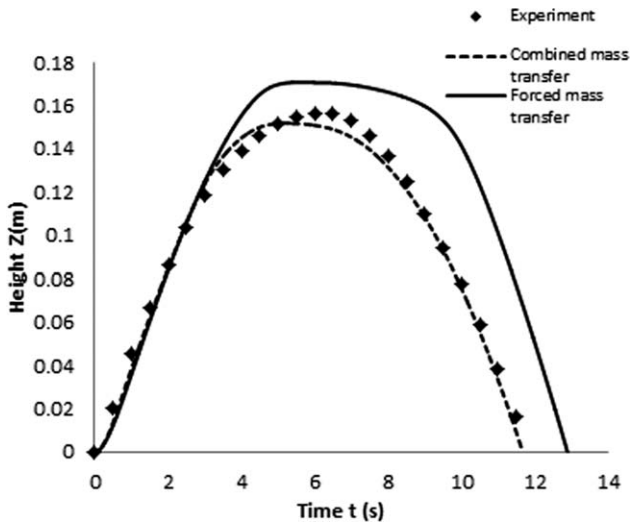


**Figure 7. Significance of combined mass transfer during stationary stage (initial mixture density = 950 kg/m$^3$).**

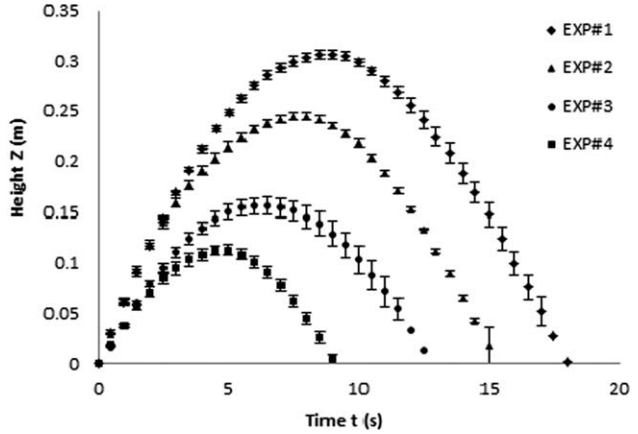


**Figure 8. Trajectories of droplets observed in the experiment.**

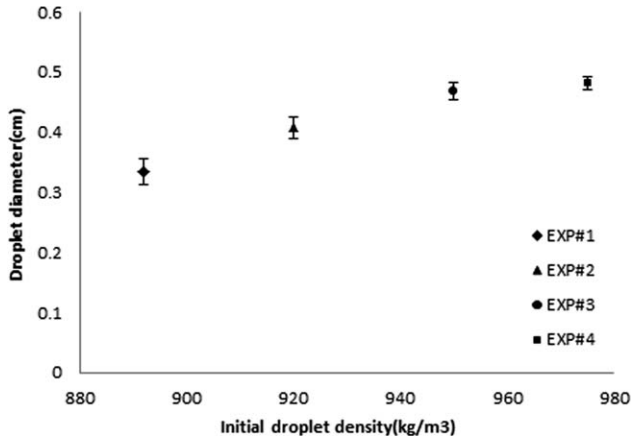


**Figure 9. Droplet sizes at the time of pinch off for mixtures injected at different initial densities.**

The significance of natural convection during stationary stage can be understood from Figure 7, which compares the trajectories of droplet obtained from numerical model by considering mass transfer to occur purely by forced convection mechanism (Eq. 14) and the one where mass loss from the droplet is dictated by Eqs. 14 and 13 (diffusion + natural convection + forced convection). The latter case with combined mass-transfer mechanism yields a trajectory curve which is in good agreement with that from the experiment. This is observed because the mass transfer during stationary stage occurs due to diffusion and natural convection. However, when the mass transfer is assumed to occur by correlation given by Eq. 14, during stationary stage, the mass lost by droplet is purely due to diffusion. So, the rate at which the mass is lost is much smaller than that observed for combined mass-transfer case. Consequently, droplet in simulation is able to reach a higher elevation and stay at the position for a much longer time. Thus, it can be concluded that natural convection enhances mass transfer over diffusion and plays in important role when droplet passes through a stationary stage.

## Results

### *Experimental*

Figure 8 depicts the trajectories of droplets released with different initial mixture densities in the experiment. The

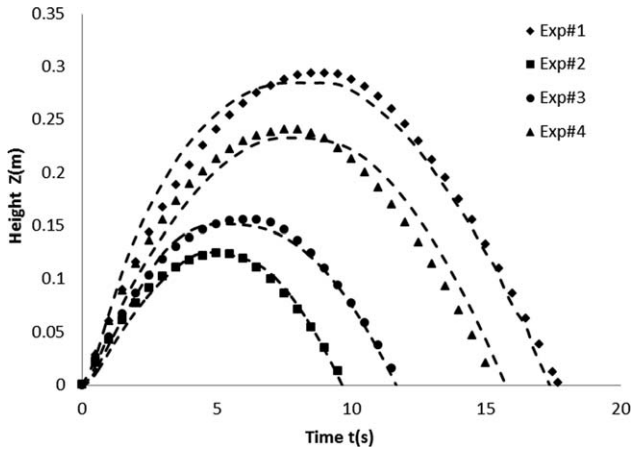


**Figure 10. Trajectory predicted by CFD model compared to that observed in experiment (dashed lines are from CFD simulations).**

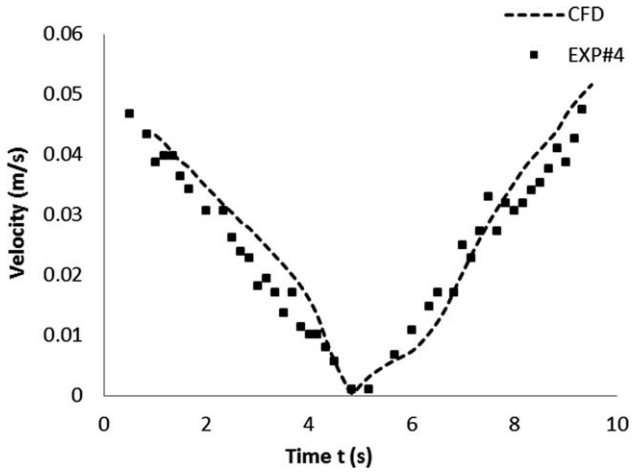


**Figure 11. Velocity Magnitude predicted of the droplet (Exp#4).**

starting density of the droplet is varied between 890 and 975 kg/m$^3$. It is observed that the droplets with lower initial mixture density are smaller in size and attain a higher level than the droplets with higher initial mixture density. The lower density difference between surrounding fluid and droplet, and the high rate of mass transfer, which is attributed to the larger interfacial area, causes the droplet with higher initial mixture density to attain a much smaller elevation at the end of ascent stage. The droplets in the experiment were able to maintain the spherical shape during the ascent as well as descent stages and did not exhibit shape oscillations.

The effect of initial mixture density on the size of droplet formed at the nozzle has been depicted in Figure 9. It can be observed that size of the droplet pinching off from nozzle increases with increase in the initial density of the mixture being injected. The pinch off mechanism of droplet is governed by the balance between the interfacial tension forces and buoyancy. With increase in the mixture density, the buoyant force required to offset the existing interfacial tension forces is achieved only when droplets grows to the larger size. In the present study, we have not studied the pinch off mechanism in detail and the focus has been on the different regimes that the droplet passes through after it pinches off from the nozzle. Because of the continuous loss to acetonitrile, a net force always acts on the droplet which is in motion and hence droplet is subjected to either acceleration or deceleration.

### *Numerical results*

A region equivalent to the size of the droplet observed in the experiment was marked in the computational domain and assigned a value of $\alpha=1$, to represent the dispersed phase. The initial mass fraction of acetonitrile in the droplet was

**Table 5. Reduction in Droplet Size Because of Mass Transfer from the Experiment**

| Density (kg/m$^3$) | Initial Droplet Diameter (mm) | Final Droplet Diameter (mm) | % Reduction |
|---|---|---|---|
| 890 | 3.30 | 2.98 | 9.69 |
| 920 | 4.10 | 3.61 | 12.02 |
| 950 | 4.65 | 4.25 | 8.66 |
| 975 | 4.90 | 4.65 | 7.55 |

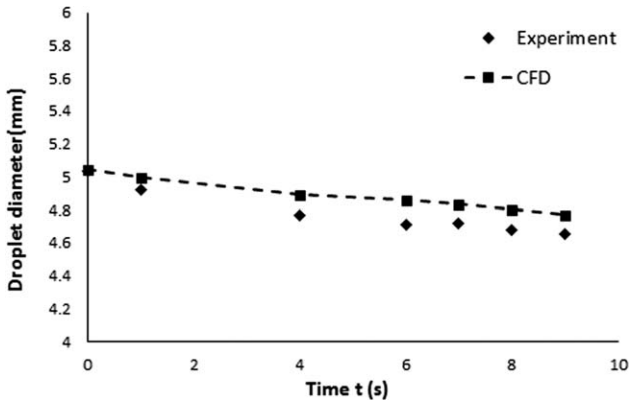


**Figure 12. Prediction of reduction in droplet size from CFD model.**

fixed according to values of $x_0$ (Table 2); the continuous phase was free from acetonitrile. Thus, the droplet was allowed to start from the rest and it lost acetonitrile in accordance to the imposed mass-transfer rate, as it traveled in the water column.

Figure 10 shows comparison between the instantaneous positions of droplet observed in the experiment with that predicted from the model. The agreement was found to be good with a deviation of less than 15%. Figure 11 shows comparison of the droplet velocities obtained from the CFD model with those observed during the experiment; the match between the velocities was found to be satisfactory. The close agreement of these results with the experimental observations suggests that the model is capable of predicting the unsteady mass transfer occurring at the interface of the droplet.

The droplet also witnesses overall reduction in its size at the end of the descent phase, due the loss of acetonitrile to the continuous phase. The data from the experiment have been tabulated in Table 5. The reduction for various droplets observed in the experiment was under 12%. In CFD model, the variation in droplet size is captured by inclusion of the source term on the right-hand side of Eq. 7, which accounts for the mass transfer. Figure 12 shows the decrease in size of droplet in Exp#4 and confirms the capability of the CFD model in correctly predicting the trend.

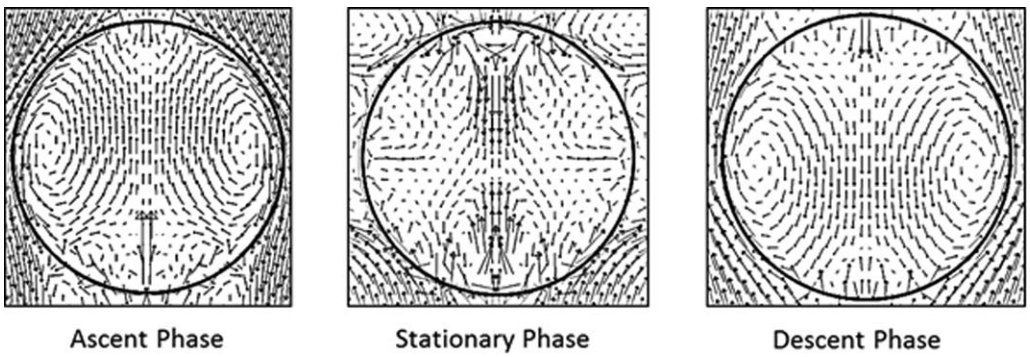


**Figure 13. Internal circulations inside the droplet at different stages; velocity vector field is relative to droplet motion.**

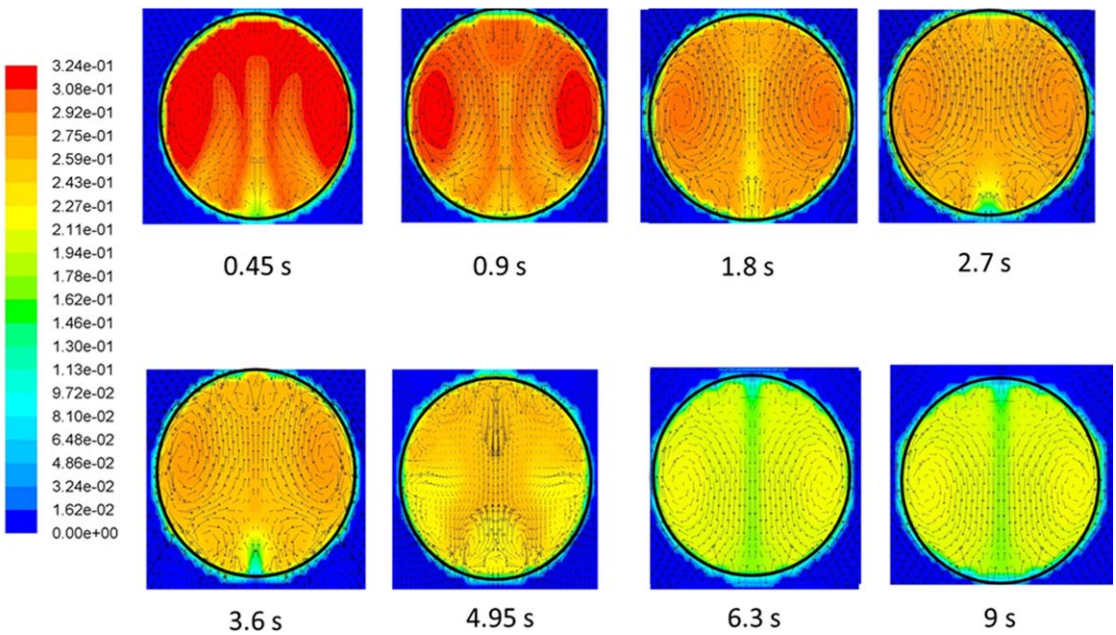


**Figure 14. Contours of mass fraction of acetonitrile inside the droplet at different instants of time.**

**[Color figure can be viewed in the online issue, which is available at wileyonlinelibrary.com.]**

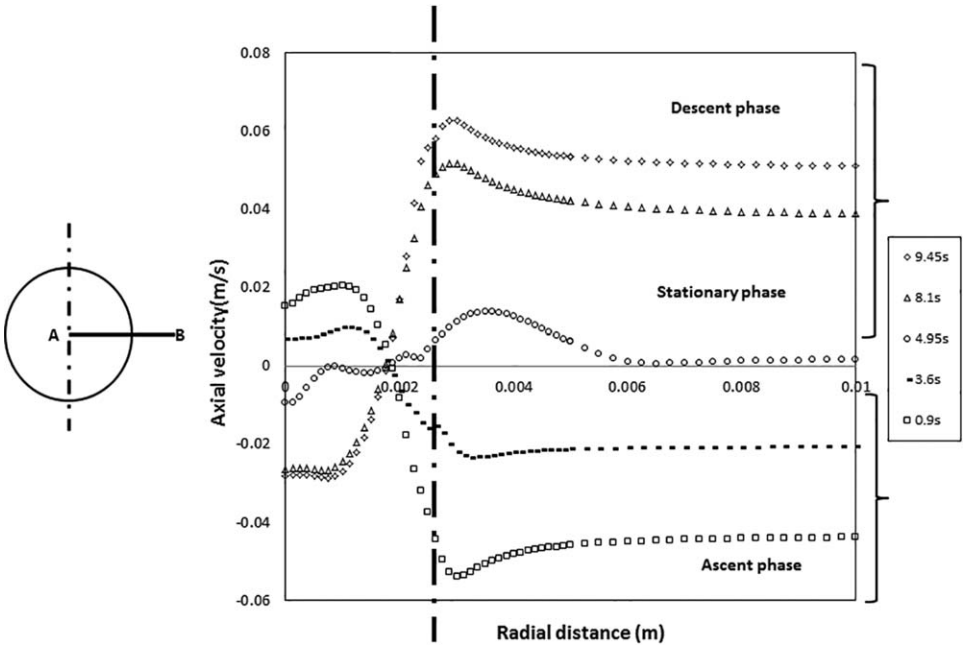


**Figure 15. Axial velocity profiles along the line AB passing through the center of the droplet.**

### *Effect on dynamics of droplet*

The change in dynamics of droplet as it moves in the water column can be noticed in Figure 13 which reveals the velocity vectors inside the droplet at different stages. Internal circulations have been depicted by constructing velocity vector field relative to average velocity of the droplet, that is, at any instant of time, the velocity with which the droplet travels in determined and is subtracted from the velocity field obtained by solving Eqs. 2 and 3. As soon as the droplet acquires motion, the shear acting at liquid–liquid interface, due to the relative motion between the dispersed and continuous phase leads to the development of internal circulations inside the droplet. With mass transfer of acetonitrile, the net buoyant force on the droplet reduces and this decelerates the droplet and hence the strength of internal circulation falls. Eventually, the internal circulations die down when the droplet passes through stationary phase. As droplet begins to acclerate, at inception of the descent phase, the internal circulations again develop but in opposite direction. The internal convection along with the diffusion influences the acetonitrile distribution inside the droplet. The concentration profiles inside the droplet at different instants of time have been shown in Figure 14.

The change in flow pattern inside and outside the droplet can be more elaborately explained through Figure 15, which depicts the axial velocity at different instants of time, along the cut-line AB which lies on the equatorial plane and passes through the center of droplet. The velocity profiles have been obtained relative to the droplet's motion. The vertical dashed line in the plot gives an approximate position of the interface. During initial stages, the axial velocities(for $t = 0.9$ s) in the regions inside the droplet along the cut-line bear a positive value. With droplet as a reference, the surrounding fluid is seen to flow in direction opposite to droplets motion and hence the axial velocities outside the droplet possess negative values. As the droplet decelerates, the strength of internal circulations drop, which can be noticed for the curve at $t = 3.6$ s. The existence of velocities near the interface outside the droplet (region right to the dashed line) confirms the presence of convection currents around the droplet which assists the overall mass transfer. As it has been mentioned earlier, during this stage mass transfer depends on the diffusion and forced convection.

The curve at $t = 4.95$ s respresents the stationary stage, where droplet comes to rest. It can be observed that the velocities disappear (also see Figure 14) at all places except in the region close to interface outside the droplet. As mentioned in earlier sections, this velocity is due to the rising mass of lighter acetonitrile-water mixture present outside the droplet. Though the droplet is stationary, the rising mass causes fluid motion around the interface, and this influences the rate at which mass transfer occurs. This provides evidence for the existence of natural convection around the droplet. Beyond $t = 4.95$ s, the droplet begins to sink and the

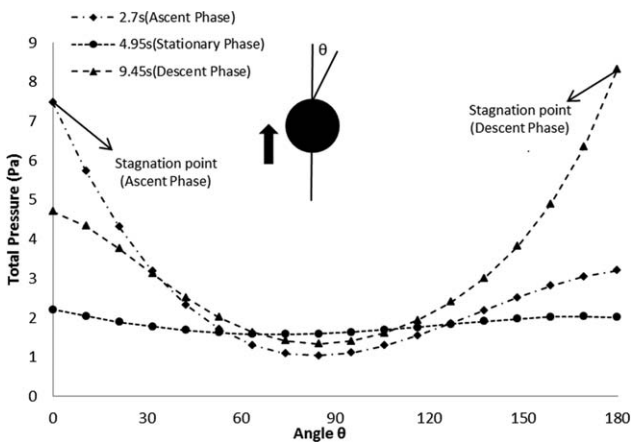


**Figure 16. Surface pressure variation for droplet with initial mixture density = 970 kg/m3 at 2.7 s (ascent stage), 4.95 s (stationary stage), and 9.5 s(descent stage).**

the internal circulations now exist in a direction opposite to that found during ascent stage.

Figure 16 shows the variation in the total surface pressure across the droplet. The curve at 2.7, 4.95, and 9.45 s represent the ascent, stationary, and descent stages, respectively. The angle is measured from the upper pole of the droplet. It can be seen that during the ascent stage the stagnation point lies at the top. The lowest pressure is observed at the equatorial plane (marked by 90°). During stationary stage, when the velocities die down, the pressure distribution around the surface of droplet is fairly uniform. However, when droplet starts descending the stagnation point shifts to the lower end of the droplet.

## Conclusions

Experimental and numerical investigations have been conducted to analyze the influence of unsteady mass transfer on the dynamics of the droplet. An organic droplet composed of a component miscible in water and an immiscible component, is generated and the droplet is released into the quiescent pool of water. The initial mixture density at the time of droplet release is less than that of water. The continuous decrease in the density of droplet due to the mass transfer of lighter miscible component, allows it pass through an ascent, stationary, and descent stages.

It is observed that different mechanisms control mass transfer of solutes as the droplet rises and sinks in the water column. During the ascent stage and descent stage mass transfer is influenced by the forced convection of surrounding fluid around the droplet. However, by the time droplet approaches the stationary stage the flow patterns inside and outside droplet change significantly and the mass-transfer rate during this stage depends on the natural convection as well as diffusion. Thus, this study has paved the way to identify the dominant mechanisms that dictate mass transfer during different stages of the droplet motion. A correlation, capable of predicting the mass transfer occurring at different stages of droplet motion has also been developed.

In addition to experimental work, a CFD model based on axisymmetric assumption has also been developed. VOF method with piecewise linear approach for interface (PLIC) construction was used to track interface between continuous and dispersed phases and the species profiles inside and outside the droplet was evaluated by including species transport equation in the model. The results derived from the CFD model are found to be in good agreement with the experimental observations and provide insight in understanding the dynamics of droplet.

## Acknowledgments

The present work has been supported by a grant from Gulf of Mexico Research Initiative (GoMRI) to the CMEDS consortium. The supercomputing facility at HPC, Louisiana State University and Louisiana Optical Network Initiative (LONI), and Extreme Science and Engineering Discovery Environment (XSEDE) is acknowledged.

### Notation

$A_d$ = surface area of the droplet, $m^2$
$c_i$ = mass concentration of acetonitrile, $kg/m^3$
$d$ = droplet diameter, m
$D_{i,j}$ = molecular diffusivity; $i$ = of the acetonitrile, $J$ = water (continuous phase), $j$ = chlorobenzene (dispersed phase), $m^2/s$
$D^*$ = diffusivity ratio $\left(D_{i,d}/D_{i,c}\right)$
$F$ = external volumetric body force, $N/m^3$
$k_l$ = overall mass-transfer coefficient, m/s
$m$ = mass of the droplet, kg
$S$ = volumetric mass-transfer rate, $kg/m^3$ s
$x$ = mass fraction of solute acetonitrile
$u$ = velocity of the droplet, m/s
$\vec{v}$ = velocity field vector, m/s
$V_d$ = volume of the droplet, $m^3$

### Greek letters

$\alpha$ = volume fraction function
$\gamma$ = surface curvature
$\rho$ = density, $kg/m^3$
$\Delta\rho$ = density difference between the phases, $kg/m^3$
$\mu$ = viscosity, kg/m s
$\mu^*$ = viscosity ratio $[\mu_d/\mu_c]$
$\sigma$ = interfacial tension, N/m

### Subscripts

c = continuous phase
d = dispersed phase
$o$ = initial value of a specified property
$r$ = radial direction
$z$ = axial direction

### Dimensionless numbers

$Ci$ = circulation number
$Re$ = Reynolds number, $\frac{du\rho_c}{\mu_c}$
$Sc$ = Schmidt number, $\frac{\mu_c}{\rho_c D_c}$
$Sh$ = Sherwood number, $\frac{k_l d}{D_c}$
$We$ = Weber number, $\frac{\rho u^2 d}{\sigma}$
$Pe$ = Peclet number, $\frac{ud}{D_c}$
$Gr$ = Grashoff number, $\frac{\Delta\rho \cdot \rho_c \cdot g d^3}{\mu_c^2}$

## Literature Cited

1. Yvon-Lewis SA, Hu L, Kessler J. Methane flux to the atmosphere from the deepwater horizon oil disaster. *Geophys Res Lett*. 2011; 38(1):L01602.
2. Clift R, Grace JR, Weber ME. *Bubbles, Drops, and Particles*. Mineola, NY: Dover Publications, 2005.
3. Bäumler K, Wegener M, Paschedag AR, Bänsch E. Drop rise velocities and fluid dynamic behavior in standard test systems for liquid/liquid extraction—experimental and numerical investigations. *Chem Eng Sci*. 2011;66(3):426–439.
4. Wegener M, Paschedag AR. The effect of soluble anionic surfactants on rise velocity and mass transfer at single droplets in systems with Marangoni instabilities. *Int J Heat Mass Transf*. 2012;55(5–6):1561–1573.
5. Kronig R, Brink JC. On the theory of extraction from falling droplets. *Flow Turbul Combust*. 1951;2(1):142–154.
6. Wesselingh JA, Bollen AM. Single particles, bubbles and drops: their velocities and mass transfer coefficients. *Chem Eng Res Des*. 1999;77(2):89–96.
7. Kumar A, Hartland S. Correlations for prediction of mass transfer coefficients in single drop systems and liquid–liquid extraction columns. *Chem Eng Res Des*. 1999;77(5):372–384.
8. Heertjes PM, Holve WA, Talsma H. Mass transfer between isobutanol and water in a spray-column. *Chem Eng Sci*. 1954;3(3):122–142.
9. Skelland AHP, Minhas SS. Dispersed phase mass transfer during drop formation and coalescence in liquid-liquid extraction. *AIChE J*. 1971;17(6):1316–1324.
10. Hashem MA, El-Bassuoni AA. Drop formation mass transfer coefficients in extraction columns. *Theor Found Chem Eng*. 2007;41(5): 506–511.
11. Humphrey JAC, Hummel RL, Smith JW. Note on the mass transfer enhancement due to circulation in growing drops. *Chem Eng Sci*. 1974;29(6):1496–1500.
12. Davidson MR, Rudman M. Volume-of-fluid calculation of heat or mass transfer across deforming interfaces in two-fluid flow. *Numer Heat Transf B Fund*. 2002;41(3–4):291–308.
13. Deshpande KB, Zimmerman WB. Simulation of interfacial mass transfer by droplet dynamics using the level set method. *Chem Eng Sci*. 2006;61(19):6486–6498.
14. Skelland AHP, Wellek RM. Resistance to mass transfer inside droplets. *AIChE J*. 1964;10(4):491–496.
15. Garner FH, Foord A, Tayeban M. Mass transfer from circulating liquid drops. *J Appl Chem*. 1959;9(6):315–323.

16. Michaelides E. *Particles, Bubbles and Drops: Their Motion, Heat and Mass Transfer*. Singapore: World Scientific, 2006.
17. Hirt CW, Nichols BD. Volume of fluid (VOF) method for the dynamics of free boundaries. *J Comput Phys*. 1981;39(1):201–225.
18. Harlow FH, Welch JE. Numerical calculation of time-dependent viscous incompressible flow of fluid with free surface. *Phys Fluids*. 1965;8(12):2182–2189.
19. Unverdi SO, Tryggvason G. A front-tracking method for viscous, incompressible, multi-fluid flows. *J Comput Phys*. 1992;99(1):180.
20. Osher S, Sethian JA. Fronts propagating with curvature-dependent speed: algorithms based on Hamilton-Jacobi formulations. *J Comput Phys*. 1988;79(1):12–49.
21. Wang J, Lu P, Wang Z, Yang C, Mao Z-S. Numerical simulation of unsteady mass transfer by the level set method. *Chem Eng Sci*. 2008;63(12):3141–3151.
22. Petera J, Weatherley LR. Modelling of mass transfer from falling droplets. *Chem Eng Sci*. 2001;56(16):4929–4947.
23. Marschall H, Hinterberger K, Schüler C, Habla F, Hinrichsen O. Numerical simulation of species transfer across fluid interfaces in free-surface flows using OpenFOAM. *Chem Eng Sci*. 2012;78:111–127.
24. Brackbill JU, Kothe DB, Zemach C. A continuum method for modeling surface tension. *J Comput Phys*. 1992;100(2):335–354.
25. Adekojo Waheed M, Henschke M, Pfennig A. Mass transfer by free and forced convection from single spherical liquid drops. *Int J Heat Mass Transf*. 2002;45(22):4507–4514.
26. Paschedag AR, Piarah WH, Kraume M. Sensitivity study for the mass transfer at a single droplet. *Int J Heat Mass Transf*. 2005; 48(16):3402–3410.
27. National Commission on BP Deepwater Horizon Oil Spill and Offshore Drilling (U.S.). *Deep water: the Gulf oil disaster and the future of offshore Drilling*. *Washington D.C., 2011*.
28. Reddy RK, Rao A, Yu Z, Wu C, Nandakumar K, Thibodeaux L, Valsaraj KT. Challenges in and approaches to modeling the complexities of deep water oil and gas release. *Oil Spill Remediation: Colloid Chemistry-Based Principles and Solutions*. Hoboken, New Jersey: Wiley, 2014.
29. French-McCay DP. Oil spill impact modeling: development and validation. *Environ Toxicol Chem*. 2004;23(10):2441–2456.
30. Rajan SM, Heideger WJ. Drop formation mass transfer. *AIChE J*. 1971;17(1):202–206.
31. Heideger WJ, Wright MW. Liquid extraction during drop formation: effect of formation time. *AIChE J*. 1986;32(8):1372–1376.
32. Heertjes PM, de Nie LH. The mechanism of mass transfer during formation, release and coalescence of drops. Part I—mass transfer to drops formed at a moderate speed. *Chem Eng Sci*. 1966;21(9):755–768.
33. Popovich AT, Lenges J. Experimental study of mass transfer during single drop formation, release and fall. *Warme-und Stoffubertragung*. 1971;4(2):87–92.
34. Young DL. Time-dependent multi-material flow with large fluid distorition. In: Morton KW, Baines MJ, editors. *Numerical Methods for Fluid Dynamics*. New York: Academic Press, 1982:273–285.
35. van Sint Annaland M, Deen NG, Kuipers JAM. Numerical simulation of gas bubbles behaviour using a three-dimensional volume of fluid method. *Chem Eng Sci*. 2005;60(11):2999–3011.
36. Scardovelli R, Zaleski S. Direct numerical simulation of free-surface and interfacial flow. *Annu Rev Fluid Mech*. 1999;31(1): 567–603.
37. Langmuir I. The evaporation of small spheres. *Phys Rev*. 1918; 12(5):368–370.
38. Schiller L, Naumann A. Fundamental calculations in gravitational processing. *Zeitschrift Des Vereines Deutscher Ingenieure*. 1933;77: 318–320.

## Appendix

The model for estimating mass-transfer correlation is described briefly

$$\frac{d}{dt}\left(\frac{V_{\mathrm{d}}\ \rho_m}{A_{\mathrm{d}}}\right)=\mathrm{k}_l\ \rho_m(x_{i,\mathrm{d}}-x_{i,\mathrm{c}}) \tag{A1}$$

The mass conservation is given by Eq. A1, states that the rate of change in mass of the droplet is solely due to the mass transfer of acetonitrile. Here, $V_{\mathrm{d}}$ represents the volume of the droplet, $A_{\mathrm{d}}$ is the interfacial area available for the mass transfer. $\mathrm{k}_l$ refers to the overall mass transfer coefficient, $x_{i,\mathrm{d}}$ and $x_{i,\mathrm{c}}$ are the mass fraction of the acetonitrile in droplet and water, respectively. The volume of water surrounding the droplet phase is far greater than the droplet volume, so the concentration of acetonitrile $x_{i,\mathrm{c}}$ in water assumes a very small value and can be safely taken equal to zero. $\rho_m$ represents the mixture density of the droplet which is given by

$$\rho_m=\frac{\rho_{\mathrm{ACN}}\rho_{\mathrm{CB}}}{\rho_{\mathrm{CB}}\left(1-x_{i,\mathrm{d}}\right)+\rho_{\mathrm{ACN}}x_{i,\mathrm{d}}} \tag{A2}$$

where $\rho_{\mathrm{ACN}}$, $\rho_{\mathrm{CB}}$ are densities of acetonitrile and chlorobenzene, respectively. The solution to Eq. A1 gives the instantaneous value of $x_{i,\mathrm{d}}$ from which $\rho_m$ can be calculated using Eq. A2.

Equation A3 represents the momentum equation which gives the force balance around the droplet(see Figure 2b)

$$m\frac{du_z}{dt}=F_D+F_G-F_B$$

$$m\frac{du_z}{dt}=F_D+V_{\mathrm{d}}\rho_m g\ -\ \rho_f V_{\mathrm{d}} g \tag{A3}$$

$$\frac{dz}{dt}=-u_z \tag{A4}$$

$F_D$ accounts for the drag force acting on the droplet which is evaluated using

$$F_D=\frac{1}{2}C_D\rho_{\mathrm{d}}U^2A \tag{A5}$$

where $A$ represents the projected area of the droplet. Schiller–Naumann correlation[38] was used for evaluating $C_D$.The instantaneous value of $\rho_m$ obtained in Eq. A2 is used in Eq. A3 to evaluate $u_z$. The solution to Eq. A4 gives the position of the droplet.

*Manuscript received Dec. 14, 2013, and revision received July 16, 2014.*